Chin. J. Astron. Astrophys. Vol. 6 (2006), No. 4, 495–502
(*http://www.chjaa.org*)

Chinese Journal of
Astronomy and
Astrophysics

Image Field Deformation of LAMOST due to Differential Atmospheric Refraction *

Jin-Ling Li, Bo Zhang, Yong Yu, Zhao-Xiang Qi and Ming Zhao

Shanghai Astronomical Observatory, Chinese Academy of Sciences, Shanghai 200030; *jll@shao.ac.cn*

Received 2005 August 18; accepted 2005 September 29

Abstract A vectorial expression of the image field deformation of LAMOST due to the differential atmospheric refraction is presented. The calculated results are compared with those from previous analyses based on the traditional spherical trigonometric formulas. It is demonstrated that different tangential displacements of star images during the observation tracking given by various authors are simply due to different reference points adopted. It is pointed out that the observational celestial pole is the center of the apparent diurnal motion, that, by referring to the observational celestial pole, the effect of the differential refraction on the image field of LAMOST during the 1.5-hour tracking period is approximately equivalent to a constant rotation of $-13.65''$ for all declination belts. It is therefore unnecessary to design a particular tracking velocity for each observation, and this will be obviously advantageous to the observation implementation. If the maximum tracking error of the fibers is $0.2''$, then the fibers are required to be able to re-position during observational tracking for sky regions south of declination $+20^\circ$ and north of declination $+60^\circ$.

Key words: telescopes — atmospheric effects — methods: analytical — methods: statistical — astrometry

1 INTRODUCTION

The issue concerning image field deformation of LAMOST due to differential atmospheric refraction has been discussed previously (Su & Wang 1997; Lu & Li 1999; Sun & Hu 1997) (Hereafter referred as paper 1 through 3). In these discussions more or less the same spherical trigonometric formulas are adopted and the radial and tangential displacements of the star images during a 1.5-hour tracking are calculated. The results given by the different authors are well consistent with one another as regards the radial component, but are not so for the tangential components. All the previous discussions adopted the traditional spherical trigonometric formulas. In contrast to these, the vectorial expression is compact, isotropic and of high precision, and the modular expression of formulas is especially convenient for computer programming. In this paper the vectorial expression of formulas is adopted and the calculated results are compared with the previous discussions. It is demonstrated that the difference is due to the different reference points adopted, and the image field deformation is directly related to the strategic design and the final effectiveness of the fiber tracking of LAMOST.

* Supported by the National Natural Science Foundation of China.

2 VECTORIAL EXPRESSION OF THE IMAGE FIELD DEFORMATION DUE TO DIFFERENTIAL ATMOSPHERIC REFRACTION

For convenience we adopt the following conventions and symbols in the derivation of the formulas.

- $\boldsymbol{S}_j$ — the airless direction vector of object. $j = 0$, i, p and z represent respectively the apparent direction vector of (a) the center of field of view (FOV) and (b) object i in the true equatorial coordinate system, (c) the true direction vector of the celestial pole, (d) the direction vector of zenith in the true equatorial coordinate system.
- $\boldsymbol{S}'_j$ — the observational direction vector of j containing the influence of atmospheric refraction.
- $[H]$ — the local hour angle coordinate system, which is right-handed with the first axis pointing to the point of intersection of the local meridian circle and the instantaneous true equator, the third to the true celestial pole.

The atmospheric refraction turns $\boldsymbol{S}_j$ into $\boldsymbol{S}'_j$, $\boldsymbol{S}'_j$ is between $\boldsymbol{S}_j$ and $\boldsymbol{S}_z$, the three are coplanar vectors, and we have

$$\boldsymbol{S}'_j = \frac{1}{\sin z_j} \left\{ sin(z_j - R_j)\boldsymbol{S}_j + \sin R_j \boldsymbol{S}_z \right\}, \tag{1}$$

where z_j is the apparent zenith distance, which is defined as the angle between the instantaneous direction vector $\boldsymbol{S}_z$ of the zenith and the apparent direction vector $\boldsymbol{S}_j$ of the object j (traditionally called the true zenith distance. For consistency of terminology, in this paper the zenith distance corresponding to the apparent direction is called the apparent zenith distance and the one corresponding to the observational direction is called the observational zenith distance). R_j is the angle of atmospheric refraction, expressed by

$$R_j = k_1 \tan(z_j - R_j) - k_2 \tan^3(z_j - R_j). \tag{2}$$

For the standard atmosphere, $k_1 = 60.3''$ and $k_2 = 0.06688''$, the corresponding refraction angle is R_j^0. When the apparent zenith distance is known, R_j^0 can be iteratively solved from Equation (2). If the local atmospheric condition departs significantly from the standard atmosphere, then the true refraction angle should be calculated by

$$R_j(T, P) = R_j^0 \times \frac{P(mb)}{1013.25} \times \frac{273.15}{273.15 + T(^\circ\mathrm{C})}, \tag{3}$$

where T and P are the air temperature and pressure at the time of observation. The vectorial expression of the apparent zenith distance is

$$z_j = \arccos(\boldsymbol{S}_z \cdot \boldsymbol{S}_j). \tag{4}$$

In the local hour angle coordinate system $[H]$, the apparent direction vector of the object is expressed as

$$\boldsymbol{S}_j = [H] \begin{bmatrix} \cos t_j \cos \delta_j \\ -\sin t_j \cos \delta_j \\ \sin \delta_j \end{bmatrix}. \tag{5}$$

If $j = p$ then $\delta_p = 90^\circ$, if $j = z$ then $t_z = 0$ and $\delta_z = \varphi$, φ is the instantaneous astronomical latitude of the observing station. From Equations (1)–(5) the observation direction $\boldsymbol{S}'_j$ can be deduced.

To describe the position of the object relative to the FOV center, a spherical polar coordinate system $S'_o - \rho\theta$ is introduced, with origin at the FOV center. As shown in Figure 1, ρ is the arc length between the object image and the FOV center and is called the radial (angular) distance from the center; θ is the field angle between the object image and the north celestial pole as seen from the FOV center, and is called the tangential (angular) distance.

The polar coordinates of the image of the object i are determined by

$$\rho_i = \arccos(\boldsymbol{S}'_o \cdot \boldsymbol{S}'_i), \tag{6}$$

$$\theta_i = \angle S'_i S'_o S_p = \arccos(\boldsymbol{T}_i \cdot \boldsymbol{T}_p), \tag{7}$$

and

$$\theta_i = \angle S'_i S'_o S_p = 2\pi - \arccos(\boldsymbol{T}_i \cdot \boldsymbol{T}_p). \tag{8}$$

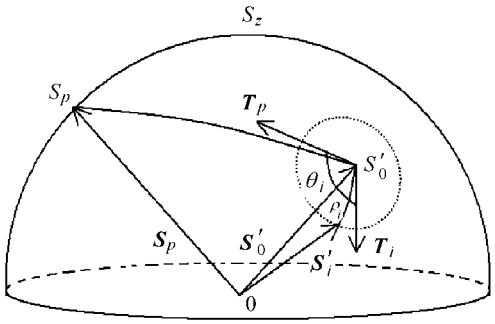

Fig. 1 Spherical polar coordinates at the FOV center.

Within the tangential plane at S'_o, Equation (7) corresponds to $\boldsymbol{T}_i$ being to the left of $\boldsymbol{T}_p$ and Equation (8) to $\boldsymbol{T}_i$ to the right of $\boldsymbol{T}_p$, where

$$\begin{aligned} \boldsymbol{T}_i &= \langle(\boldsymbol{S}'_o \times \boldsymbol{S}'_i) \times \boldsymbol{S}'_o\rangle, \\ \boldsymbol{T}_p &= \langle(\boldsymbol{S}'_o \times \boldsymbol{S}_p) \times \boldsymbol{S}'_o\rangle\,. \end{aligned} \tag{9}$$

These are respectively the tangential vectors of the great circle $\widehat{S'_oS'_i}$ and $\widehat{S'_oS_p}$ at S'_o. $\langle\boldsymbol{S}\rangle$ represents the unit vector of $\boldsymbol{S}$, S'_i and S_p are the orientation points of $\boldsymbol{S}'_i$ and $\boldsymbol{S}_p$.

3 A COMPARISON WITH THE CALCULATIONS OF PAPER 2

According to the vectorial expressions introduced above we calculate the polar coordinates (ρ_i, θ_i) of some postulated object images with the hour angle of the FOV center set at $-45^{\rm m}$, 0 and $+45^{\rm m}$, and then determine the displacement $(\Delta\rho_i, \Delta\theta_i)$ of the image at $\pm45^{\rm m}$ relative to 0. The configuration of the postulated images is shown in Figure 2 and the astronomical latitude of the observation site is set at $\varphi = 40.4^\circ$. Because the radial displacement $\Delta\rho_i$ calculated in this paper is in accordance with those of other authors within the computing precision, we just list in Table 1 the tangential angular displacement $\Delta\theta_i$. The corresponding results of paper 2 are also listed for comparison. Though paper 3 does not provide the tangential angular displacement data, it can be judged from the figures and the statistics that the authors of paper 3 have obtained the same data as in paper 2.

From Table 1 it is clear that within the declination belt $[-10^\circ, +80^\circ]$ our calculations are in good agreement with those of paper 2. However, paper 2 provides no data for sky regions above declination 80°. So here, we extend our calculation to declinations 85°, 89° and 90°, and the results are also listed in Table 1. It shows that as the declination increases, the angular displacement grows sharply and finally equals the diurnal motion at declination 90°.

4 COMPARISON WITH THE CALCULATIONS OF PAPER 1

In the calculation of the tangential displacement, paper 1 refers to the northernmost star on the edge of the FOV , which differs from paper 2 which refers to the north celestial pole. In order to certify the calculations of paper 1, let $\boldsymbol{T}_p$ in Equations (7) and (8) be replaced by $\boldsymbol{T}_1$, representing a guide star as the reference point rather than the north celestial pole, that is

$$\theta'_i = \angle S'_iS'_oS'_1 = \arccos(\boldsymbol{T}_i \cdot \boldsymbol{T}_1), \tag{10}$$

and

$$\theta'_i = \angle S'_iS'_oS'_1 = 2\pi - \arccos(\boldsymbol{T}_i \cdot \boldsymbol{T}_1), \tag{11}$$

where

$$\boldsymbol{T}_1 = \langle(\boldsymbol{S}'_o \times \boldsymbol{S}'_1) \times \boldsymbol{S}'_o\rangle\,. \tag{12}$$

Table 1 Tangential Angular Displacement of Star Images Due to The Differential Atmospheric Refraction ($\Delta\theta$, Referring to The True Celestial Pole) (Unit: arcsec)

	1	2	3	4	5	6	7	8
$\delta = -10^\circ$, FOV$= 5^\circ$				$-45^{\rm m}$ local hour angle of FOV center				
Paper 2	-18.57	-2.42	14.82	-2.73	-21.73	-2.51	15.31	-2.33
This paper	-18.61	-2.43	14.82	-2.72	-21.74	-2.52	15.31	-2.33
				$45^{\rm m}$ local hour angle of FOV center				
Paper 2	-18.65	-2.33	15.31	-2.51	-21.73	-2.73	14.85	-2.42
This paper	-18.61	-2.33	15.31	-2.52	-21.74	-2.72	14.82	-2.43
$\delta = 20^\circ$, FOV$= 5^\circ$				$-45^{\rm m}$ local hour angle of FOV center				
Paper 2	0.34	3.27	7.18	3.76	-0.67	2.73	7.29	4.35
This paper	0.30	3.26	7.18	3.76	-0.66	2.73	7.29	4.36
				$45^{\rm m}$ local hour angle of FOV center				
Paper 2	0.26	4.35	7.29	2.73	-0.67	3.76	7.18	3.27
This paper	0.31	4.36	7.29	2.73	-0.66	3.76	7.18	3.26
$\delta = 40^\circ$, FOV$= 5^\circ$				$-45^{\rm m}$ local hour angle of FOV center				
Paper 2	7.90	7.19	7.72	7.97	7.05	6.67	7.77	8.57
This paper	7.84	7.19	7.72	7.97	7.06	6.66	7.78	8.57
				$45^{\rm m}$ local hour angle of FOV center				
Paper 2	7.78	8.57	7.77	6.67	7.05	7.97	7.72	7.19
This paper	7.84	8.57	7.78	6.66	7.06	7.97	7.72	7.19
$\delta = 60^\circ$, FOV$= 5^\circ$				$-45^{\rm m}$ local hour angle of FOV center				
Paper 2	20.41	15.85	13.27	17.26	19.42	15.35	13.29	17.89
This paper	20.36	15.85	13.28	17.26	19.43	15.35	13.29	17.89
				$45^{\rm m}$ local hour angle of FOV center				
Paper 2	20.31	17.89	13.29	15.35	19.42	17.26	13.27	15.85
This paper	20.36	17.89	13.29	15.35	19.43	17.26	13.28	15.85
$\delta = 80^\circ$, FOV$= 3^\circ$				$-45^{\rm m}$ local hour angle of FOV center				
Paper 2	75.96	64.16	56.58	67.68	74.89	63.96	56.54	68.08
This paper	75.90	64.17	56.59	67.69	74.91	63.97	56.55	68.09
				$45^{\rm m}$ local hour angle of FOV center				
Paper 2	75.82	68.08	56.54	63.96	74.89	67.68	56.58	64.16
This paper	75.91	68.09	56.55	63.97	74.90	67.69	56.59	64.17
FOV$= 3^\circ$				$-45^{\rm m}$ local hour angle of FOV center				
$\delta = 85^\circ$	156.13	141.01	131.29	145.57	154.86	140.90	131.21	145.97
$\delta = 89^\circ$	776.39	757.65	745.71	763.38	774.82	757.64	745.61	763.79
$\delta = 90^\circ$	40517	40497	40484	40503	40515	40497	40484	40503
FOV$= 3^\circ$				$45^{\rm m}$ local hour angle of FOV center				
$\delta = 85^\circ$	156.13	145.97	131.21	140.90	154.86	145.57	131.29	141.01
$\delta = 89^\circ$	776.39	763.79	745.61	757.64	774.82	763.38	745.71	757.65
$\delta = 90^\circ$	40517	40503	40484	40497	40515	40503	40484	40497

With the same calculation procedure as for $\Delta\theta_i$, the resulting $\Delta\theta_i'$ is listed in Table 2 together with the calculations of paper 1 for comparison. As shown in Table 2 our $\Delta\theta_i'$ is in very good accordance with that of paper 1 within computing precision, which demonstrates the equivalence and validity of both calculations. Within the arctic zone the extremely large angular displacement as shown in Table 1 disappears, which indicates that to refer to a guide star on the edge of the FOV is a reasonable way in the calculation of the tangential displacement of the images.

It is easy to understand from Table 2 that the systematic rotation of the image field represented by the data depends directly on the choice of guide stars. Different guide stars definitely lead to different systematic rotations. However, the effect of the differential atmospheric refraction on the FOV deformation of LAMOST should be unique at a specified epoch rather than uncertain or dependent on guide stars. Both the radial and tangential displacements of star image reflect the field deformation. Perhaps the rotation of image field indicated by all the data is solely the displacement of the reference point. In order to confirm this suspicion, a further analysis is made in the next sections.

Table 2 Tangential Angular Displacement of Star Images Due to The Differential Atmospheric Refraction ($\Delta\theta'$, Referring to a Guide Star) (Unit: arcsec)

	1	2	3	4	5	6	7	8
$\delta = -10^\circ$, FOV$= 5^\circ$				$-45^{\rm m}$ local hour angle of FOV center				
Paper 1	0.00	−16.18	−33.42	−15.88	3.13	−16.09	−33.91	−16.28
This Paper	0.00	−16.18	−33.43	−15.89	3.13	−16.09	−33.92	−16.28
				$45^{\rm m}$ local hour angle of FOV center				
Paper 1	0.00	−16.28	−33.91	−16.09	3.13	−15.88	−33.42	−16.18
This Paper	0.00	−16.28	−33.92	−16.09	3.13	−15.89	−33.43	−16.18
$\delta = 20^\circ$, FOV$= 5^\circ$				$-45^{\rm m}$ local hour angle of FOV center				
Paper 1	0.00	−2.96	−6.88	−3.46	0.97	−2.43	−6.98	−4.05
This Paper	0.00	−2.96	−6.88	−3.46	0.96	−2.43	−6.99	−4.05
				$45^{\rm m}$ local hour angle of FOV center				
Paper 1	0.00	−4.05	−6.98	−2.43	0.97	−3.46	−6.88	−2.96
This Paper	0.00	−4.05	−6.99	−2.43	0.97	−3.46	−6.88	−2.96
$\delta = 40^\circ$, FOV$= 5^\circ$				$-45^{\rm m}$ local hour angle of FOV center				
Paper 1	0.00	0.65	0.12	−0.13	0.79	1.18	0.07	−0.73
This Paper	0.00	0.65	0.12	−0.13	0.79	1.18	0.07	−0.73
				$45^{\rm m}$ local hour angle of FOV center				
Paper 1	0.00	−0.73	0.07	1.18	0.79	−0.13	0.12	0.65
This Paper	0.00	−0.73	0.07	1.18	0.79	−0.13	0.12	0.65
$\delta = 60^\circ$, FOV$= 5^\circ$				$-45^{\rm m}$ local hour angle of FOV center				
Paper 1	0.00	4.51	7.06	3.10	0.93	5.01	7.07	2.47
This Paper	0.00	4.52	7.08	3.10	0.93	5.01	7.07	2.47
				$45^{\rm m}$ local hour angle of FOV center				
Paper 1	0.00	2.47	7.07	5.01	0.93	3.10	7.08	4.51
This Paper	0.01	2.47	7.07	5.01	0.94	3.10	7.08	4.51
$\delta = 80^\circ$, FOV$= 3^\circ$				$-45^{\rm m}$ local hour angle of FOV center				
Paper 1	0.00	11.74	19.31	8.21	1.01	11.93	19.36	7.81
This Paper	0.00	11.74	19.32	8.22	1.00	11.93	19.36	7.81
				$45^{\rm m}$ local hour angle of FOV center				
Paper 1	0.00	7.81	19.36	11.93	1.01	8.21	19.31	11.74
This Paper	0.00	7.81	19.36	11.93	1.01	8.22	19.32	11.74
$\delta = 90^\circ$, FOV$= 3^\circ$				$-45^{\rm m}$ local hour angle of FOV center				
Paper 1	0.00	19.82	32.39	13.72	1.67	19.79	32.51	13.31
This Paper	0.00	19.82	32.40	13.72	1.67	19.79	32.51	13.32
				$45^{\rm m}$ local hour angle of FOV center				
Paper 1	0.00	13.31	32.51	19.79	1.67	13.72	32.39	19.82
This Paper	0.00	13.32	32.51	19.79	1.67	13.72	32.40	19.82

5 THE OBSERVATIONAL DIRECTION OF THE CELESTIAL POLE

Suppose there is a star whose instantaneous true declination is 90°. The "apparent altitude" of this "north pole star" is φ as observed at the station of latitude φ. However, because of the atmospheric refraction, the "observational altitude" of this star is not exactly φ but $\varphi + R_p$, where R_p is the angle of atmospheric refraction at the north pole. We call the refracted north pole as the observational celestial pole. It is not difficult to understand that the center of the diurnal circle of observed stars should be the observational celestial pole, rather than the true celestial pole. The observational celestial pole is the fixed point of apparent diurnal motion. The direction of the true celestial pole is stationary relative to the observational celestial pole in the local hour angle and the horizontal coordinate system, but it has diurnal motion around the observational celestial pole relative to the star background. In long-time astrometric tracking and observations the field deformation should be calculated by referring to the observational celestial pole rather than the true celestial pole. It is true for not only LAMOST tracking but also for all photographic observations of long-time exposure. The field angle of a star image in the FOV referred to the observational celestial pole can be calculated in a way similar to Equations (7) and (8):

$$\beta_i = \angle S_i' S_o' S_p' = \arccos\left(\boldsymbol{T}_i \cdot \boldsymbol{T}_p'\right), \tag{13}$$

and

$$\beta_i = \angle S_i' S_o' S_p' = 2\pi - \arccos\left(\boldsymbol{T}_i \cdot \boldsymbol{T}_p'\right), \tag{14}$$

where

$$\boldsymbol{T}'_p = \langle (\boldsymbol{S}'_o \times \boldsymbol{S}'_p) \times \boldsymbol{S}'_o \rangle \,. \tag{15}$$

The corresponding calculations of $\Delta\beta_i$ are listed in Table 3, from which it is seen that, in contrast to $\Delta\theta_i$ in Table 1, in the north polar region there is no sharply increase in $\Delta\beta_i$, which indicates that compared to referring to the true celestial pole, it is more reasonable to refer to the observational celestial pole in order to describe the field deformation of LAMOST due to the differential atmospheric refraction. Which is the more reasonable, $\Delta\theta'$ or $\Delta\beta$? Equivalently, which one should be referred to, a guide star or the observational celestial pole? More comparisons and analyses are required.

Table 3 Tangential Angular Displacement of Star Images Due to The Differential Atmospheric Refraction ($\Delta\beta$, Referring to The Observational Celestial Pole) (FOV$= 5^\circ$, Unit: arcsec)

Declination	1	2	3	4	5	6	7	8
$-45^{\rm m}$ local hour angle of FOV center								
-10°	−32.61	−16.42	0.82	−16.72	−35.73	−16.51	1.31	−16.33
0°	−23.25	−13.91	−3.56	−13.72	−25.08	−14.32	−3.29	−13.18
10°	−17.84	−12.35	−5.90	−11.97	−19.09	−12.85	−5.74	−11.38
20°	−14.37	−11.41	−7.49	−10.91	−15.34	−11.94	−7.38	−10.32
30°	−11.97	−10.92	−8.85	−10.30	−12.80	−11.46	−8.78	−9.71
40°	−10.16	−10.81	−10.28	−10.03	−10.95	−11.34	−10.22	−9.43
50°	−8.66	−11.06	−12.00	−10.04	−9.48	−11.58	−11.97	−9.43
60°	−7.22	−11.73	−14.30	−10.32	−8.16	−12.23	−14.29	−9.69
70°	−5.55	−12.97	−17.61	−10.89	−6.72	−13.42	−17.63	−10.24
80°	−3.08	−15.12	−22.74	−11.78	−4.75	−15.44	−22.82	−11.11
90°	0.36	−20.09	−32.62	−14.10	−2.42	−20.04	−32.81	−13.42
$45^{\rm m}$ local hour angle of FOV center								
-10°	−32.61	−16.33	1.31	−16.51	−35.73	−16.72	0.82	−16.42
0°	−23.25	−13.18	−3.29	−14.32	−25.08	−13.72	−3.56	−13.91
10°	−17.84	−11.38	−5.74	−12.85	−19.09	−11.97	−5.90	−12.35
20°	−14.37	−10.32	−7.38	−11.94	−15.34	−10.91	−7.49	−11.41
30°	−11.97	−9.71	−8.78	−11.46	−12.80	−10.30	−8.85	−10.92
40°	−10.16	−9.43	−10.23	−11.34	−10.95	−10.03	−10.28	−10.81
50°	−8.66	−9.43	−11.97	−11.58	−9.48	−10.04	−12.00	−11.06
60°	−7.22	−9.69	−14.29	−12.23	−8.16	−10.32	−14.30	−11.73
70°	−5.54	−10.24	−17.63	−13.42	−6.72	−10.89	−17.61	−12.97
80°	−3.08	−11.11	−22.82	−15.44	−4.76	−11.78	−22.74	−15.12
90°	0.36	−13.42	−32.81	−20.04	−2.42	−14.10	−32.62	−20.09

6 JOINT ANALYSIS OF VARIOUS DATA SETS

Now we have three sets of data: (1) $\Delta\theta$, referred to the true celestial pole, (b) $\Delta\theta'$, referred to a guide star, and (c) $\Delta\beta$, referred to the observational celestial pole. Table 4 gives some statistical results of the three sets of data. Column "Average" shows the mean of the tangential angular displacements for all the postulated star images shown in Figure 2, which corresponds to the mean rotation of the image field as affected by the differential atmospheric refraction. Column "STD" describes the level of deviation of the tangential angular displacement relative to the average. Column "P2P" is the absolute sum of the maximum and minimum residual tangential displacement during the 1.5-hour tracking, which indicates that after the average rotation is applied to the image field whether or not the residual displacement is tolerable to the tracking. Column "AD (5°)" and "AD (3°)" present the angular displacement at the center of the sphere, corresponding to the peak to peak residual angular displacement at the edge of 5° and 3° FOV, respectively. Some conclusion can be deduced from the comparison of these data sets as follows:

- After the deduction of the mean rotation from the three sets of data, the residual deformations in the three datasets are completely the same. This means, as anticipated, the field deformation is unique. Figure 2 shows the residual deformation of images at the edge of 5° FOV for various declination belts.

Table 4 Some Statistical Data of the Eight Postulated Images in Fig. 2 (Unit: arcsec)

Declination	Average	STD	P2P	AD (5°)	AD (3°)
θ: referring to the true celestial pole					
−10°	−2.53	13.35	37.05	1.62	0.97
0°	0.00	7.86	21.79	0.95	0.57
10°	1.86	4.81	13.34	0.58	0.35
20°	3.53	2.85	7.95	0.35	0.21
30°	5.33	1.45	4.02	0.18	0.11
40°	7.60	0.60	1.91	0.08	0.05
50°	10.93	1.30	3.35	0.15	0.09
60°	16.59	2.63	7.08	0.31	0.19
70°	28.43	4.47	12.09	0.53	0.32
80°	65.98	7.29	19.74	0.86	0.52
90°	40500	12.24	33.18	1.45	0.87
θ': referring to a guide star					
−10°	16.08	13.35	37.05	1.62	0.97
0°	9.47	7.86	21.78	0.95	0.57
10°	5.70	4.81	13.35	0.58	0.35
20°	3.23	2.85	7.95	0.35	0.21
30°	1.37	1.45	4.02	0.18	0.11
40°	−0.24	0.60	1.91	0.08	0.05
50°	−1.87	1.29	3.34	0.15	0.09
60°	−3.77	2.63	7.08	0.31	0.19
70°	−6.34	4.47	12.09	0.53	0.32
80°	−10.28	7.29	19.74	0.86	0.52
90°	−17.25	12.24	33.18	1.45	0.87
β: referring to the observational celestial pole					
−10°	−16.52	13.34	37.04	1.62	0.97
0°	−13.79	7.86	21.79	0.95	0.57
10°	−12.14	4.81	13.35	0.58	0.35
20°	−11.14	2.85	7.96	0.35	0.21
30°	−10.60	1.45	4.02	0.18	0.11
40°	−10.40	0.60	1.91	0.08	0.05
50°	−10.53	1.29	3.34	0.15	0.09
60°	−10.99	2.63	7.08	0.31	0.19
70°	−11.88	4.47	12.08	0.53	0.32
80°	−13.35	7.29	19.74	0.86	0.52
90°	−16.89	12.23	33.17	1.45	0.87

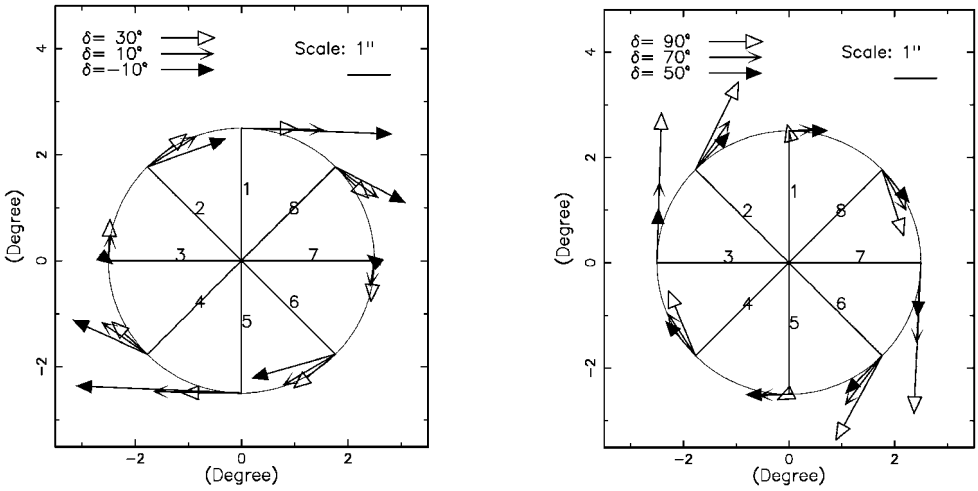

Fig. 2 Deformation of postulated images for various declination belts.

Therefore, questions such as what is the exact size of field deformation caused by the differential refraction, whether the deformation is tolerable or not and so on, are almost clarified. If the permissible error limit in the orientation of LAMOST fiber is $0.4''$, the maximum positioning error of fibers during the tracking should not be larger than $0.2''$. From Table 4 it can be concluded that the differential deformation should not be neglected for the sky regions south of declination $+20^\circ$ and north of declination $+60^\circ$. In other words, the differential refraction deformation should not be neglected for most of the observational sky regions, except for the area near the zenith. In addition, there is actually no essential difference between high-declination and low-declination region. The case naturally requires the LAMOST fibers being able to re-position during observational tracking.

- The extremely large rotation of $\Delta\theta$ within the polar region is intuitively wrong. If the tracking velocity of the focal surface is designed according to $\Delta\theta$, it is hard to actually realize the observational tracking within high declination region. To reckon the differential refraction deformation by referring to the true celestial pole is rather a regressive move.
- About $\Delta\theta'$, the mean additional rotations of different declination belts clearly differ from each other, and are directly dependent on the choice of guide stars. In the tracking mode, a guide star within the intended observation sky region should be chosen beforehand and the precise calculation should be done before the observation, and not by on-site treatment. Whenever the prospective observational condition does not materialize, the observation plan would be hard to carry on. Moreover, to control the rotation of the focal surface according to the tangential displacement of a guide star rather than the mean deformation of the image field will increase the relative tangential displacements of other stars. This is obviously unfavorable to the observational tracking.
- Concerning $\Delta\beta$, it can be seen that the mean rotation of the image field is nearly the same for all the declination belts. If the rotation is designed to be $-13.65''$ which is the mean of the maximum and minimum rotation of the image field, then the residual mean rotations at the center of the sphere for all the declination belts will be less than $0.2''$. Since the re-positioning ability of fibers is a natural prerequisite, such small residual rotations could be taken as part of the residual tangential displacement and be easily handled. Accordingly, it is unnecessary to design a particular tracking velocity for each observation, which will be obviously advantageous to the implementation of the observation.

Acknowledgements During the preparation of this paper, we have had rewarding discussions with Professor Wei Mao of Yunnan Astronomical Observatory and Professor Yifei Xia of the Astronomy Department of Nanjing University. This work is partly supported by the National Natural Science Foundation of China and Chinese Academy of Sciences.

References

Su D. Q., Wang Y. N., 1997, Acta Astrophys. Sin., 17, 202
Lu C. L., Li D. M., 1999, Acta Astron. Sin., 40, 130
Sun A. Q., Hu J. Y., 1997, Acta Astrophys. Sin., 17, 213